Published March 30, 2017

A new mechanism of voltage-dependent gating exposed by $K_V10.1$ channels interrupted between voltage sensor and pore

Adam P. Tomczak,[1] Jorge Fernández-Trillo,[1] Shashank Bharill,[3,4] Ferenc Papp,[5,6] Gyorgy Panyi,[5,6] Walter Stühmer,[2] Ehud Y. Isacoff,[3,4] and Luis A. Pardo[1]

[1]Oncophysiology Group and [2]Department of Molecular Biology of Neuronal Signals, Max Planck Institute for Experimental Medicine, 37075 Göttingen, Germany

[3]Department of Molecular and Cell Biology and [4]Helen Wills Neuroscience Institute, University of California, Berkeley, Berkeley, CA 94720

[5]Department of Biophysics and Cell Biology and [6]MTA-DE-NAP B Ion Channel Structure-Function Research Group, RCMM, University of Debrecen, 4032 Debrecen, Hungary

Voltage-gated ion channels couple transmembrane potential changes to ion flow. Conformational changes in the voltage-sensing domain (VSD) of the channel are thought to be transmitted to the pore domain (PD) through an α-helical linker between them (S4–S5 linker). However, our recent work on channels disrupted in the S4–S5 linker has challenged this interpretation for the KCNH family. Furthermore, a recent single-particle cryo-electron microscopy structure of $K_V10.1$ revealed that the S4–S5 linker is a short loop in this KCNH family member, confirming the need for an alternative gating model. Here we use "split" channels made by expression of VSD and PD as separate fragments to investigate the mechanism of gating in $K_V10.1$. We find that disruption of the covalent connection within the S4 helix compromises the ability of channels to close at negative voltage, whereas disconnecting the S4–S5 linker from S5 slows down activation and deactivation kinetics. Surprisingly, voltage-clamp fluorometry and MTS accessibility assays show that the motion of the S4 voltage sensor is virtually unaffected when VSD and PD are not covalently bound. Finally, experiments using constitutively open PD mutants suggest that the presence of the VSD is structurally important for the conducting conformation of the pore. Collectively, our observations offer partial support to the gating model that assumes that an inward motion of the C-terminal S4 helix, rather than the S4–S5 linker, closes the channel gate, while also suggesting that control of the pore by the voltage sensor involves more than one mechanism.

INTRODUCTION

Voltage-gated ion channels are crucial for the function of excitable tissues (Hille, 2001). They have a remarkable ability to switch between open and closed conformation upon transmembrane potential changes of less than 100 mV, which underlies action potentials in neurons and contraction of muscle cells. Voltage-gated channels that conduct Na^+, K^+, and Ca^{2+} share a common structural blueprint with four groups of six transmembrane helices arranged in independent subunits or a single protein with four internal repeats. The first four helices named S1 to S4 belong to the voltage-sensing domain (VSD), whereas S5 and S6 make up the pore domain (PD; Long et al., 2005a). The S4 helix has an arrangement of voltage-sensing basic residues (Stühmer et al., 1989; Papazian et al., 1991) that move across the transmembrane electric field, giving rise to gating currents (Armstrong and Bezanilla, 1973). The extent of S4 motion in voltage-gated K^+ channels has been a subject of intense debate (Gandhi et al., 2003; Jiang et al., 2003; Chanda et al., 2005; Posson et al., 2005; Ruta et al., 2005), and a consensus estimate can be found at around 10 Å (Vargas et al., 2012). VSD movement is translated into switching between permeating and nonpermeating states in the PD.

Based on the available crystal structures of voltage-gated channels (Long et al., 2005a,b, 2007; Payandeh et al., 2011), as well as a host of mutagenesis and functional experiments (Slesinger et al., 1993; Sanguinetti and Xu, 1999; Lu et al., 2002; Ferrer et al., 2006; Labro et al., 2008, 2011; Van Slyke et al., 2010), it is assumed that the conformational changes of the voltage sensor are transmitted to the pore by the α-helical linker between the S4 and S5 helices. The S4–S5 linker interacts with the channel gate in S6, constricting or dilating the channel pore. However, it is still only partially understood how this process occurs mechanistically (Chowdhury and Chanda, 2012; Isacoff et al., 2013). For instance, it is not clear whether the VSD is required

Correspondence to Luis A. Pardo: Pardo@em.mpg.de
J. Fernández-Trillo's present address is Instituto de Neurociencias, Universidad Miguel Hernández–CSIC, 03550 Alicante, Spain.
S. Bharill's present address is Affinita Biotech, South San Francisco, CA 94080.

Abbreviations used: MTSET, [2-(trimethylammonium)ethyl]methanethiosulfonate bromide; PD, pore domain; TIRF, total internal reflection fluorescence; TMRM, tetramethylrhodamine maleimide; VCF, voltage-clamp fluorometry; VSD, voltage-sensing domain.

The Rockefeller University Press $30.00
J. Gen. Physiol. 2017
https://doi.org/10.1085/jgp.201611742

Published March 30, 2017

to prevent the channel from opening at negative potentials (negative coupling between VSD and PD) or to open the channel at positive potentials (positive coupling). Pore modules of specific bacterial channels seem to prefer the open conformation in the absence of the voltage sensor (Santos et al., 2008; McCusker et al., 2011, 2012; Shaya et al., 2011; Syeda et al., 2012), whereas experimental studies in Shaker (Yifrach and MacKinnon, 2002; Pless et al., 2013) and molecular dynamics simulations predict a thermodynamic preference for the closed state (Jensen et al., 2010, 2012).

K_V10.1 (eag1, *KCNH1*) is a voltage-dependent K^+ channel implicated in tumor growth (Pardo et al., 1999; Hemmerlein et al., 2006). Its physiological roles include modulation of synaptic activity in cerebellar neurons (Mortensen et al., 2015), as well as regulation of cell cycle progression (Urrego et al., 2016) and primary cilium disassembly in proliferating cells (Sánchez et al., 2016). A recent cryo-electron microscopy (cryo-EM) structure of K_V10.1 revealed that the S4–S5 linker is a short loop, which does not allow the channel to have a domain-swapped architecture, unlike the other known K_V channel structures with a longer, helical S4–S5 linker (Whicher and MacKinnon, 2016). In the domain-swapped channels, the S4–S5 linker passes underneath the PD helices of the neighboring subunit before it connects to the S5 helix of its own subunit. In this way, the S4–S5 linkers form a ring around the S6 helices, controlling the dilation of the channel pore. In contrast, the short S4–S5 linker of K_V10.1 cannot act as a mechanical lever to gate the channel, suggesting a radically different voltage-gating mechanism. This structure agrees with our previous finding that *KCHN* family channels tolerate an interruption of the S4–S5 linker, as they assemble and remain voltage gated when VSD and PD are expressed as separate parts in *Xenopus* oocytes, forming "split" channels (Lörinczi et al., 2015). Using a series of split channels as an experimental model, we set out to investigate the novel gating mechanism in K_V10.1 and look for interactions at the interface between VSD and PD. We also took advantage of the possibility to express isolated PDs to check whether the pore intrinsically prefers the open or closed conformation.

MATERIALS AND METHODS

Mutagenesis and expression in *Xenopus* oocytes

The VSD and PD sequences of Y347 split were generated from K_V10.1 sequence in the pSGEM oocyte expression vector as previously described (Lörinczi et al., 2015). To make further VSD and PD sequences, we then removed or inserted codons by PCR-based mutagenesis. All site-directed mutagenesis was performed with the QuikChange kit (Agilent Technologies) according to the manufacturer's instructions. The N-terminal EGFP fusion proteins used in colocalization experiments were generated by PCR amplification of the relevant constructs and pasting them in the multicloning site of pGEMHE-X-EGFP vector. The N terminus of the channel was connected to the C terminus of EGFP with the following 19–amino acid linker: GGSGGSGGSGGSGGR SRSS. mCherry fusions were made with the In-Fusion kit (Takara Bio Inc.) by first cloning the relevant ORFs at the multicloning site of pmCherry-N1 vector (Takara Bio Inc.) and subcloning of the resulting fusion proteins into the oocyte expression vector pSGEM. The C terminus of the channel was connected to the N terminus of mCherry with a 6–amino acid linker: GGSGGS. DNA constructs were linearized with SfiI or NheI. cRNAs were synthesized using the T7 mMESSAGE mMACHINE kit (Ambion). To express full-length constructs, oocytes were injected with 0.05–0.5 ng RNA. To express split channels, more RNA was injected, typically 5–10 ng of each part. Before experiments, oocytes were kept at 18°C in ND-96 medium (mM: 96 NaCl, 2 KCl, 0.2 $CaCl_2$, 2 $MgCl_2$, 0.5 theophylline, and 5 HEPES, pH 7.5/NaOH). Full-length constructs usually expressed very well on the following day, whereas the functional expression of split channels required 2–3 d.

Electrophysiological recordings

2–5 d after RNA injection, membrane currents were recorded at room temperature under two-electrode voltage-clamp, using a TurboTEC 10-CD amplifier (NPI Electronics). Signals were low-pass filtered at 1.3 kHz, digitized at 10 kHz with the ITC-16 interface of EPC9 patch-clamp amplifier (HEKA), and acquired with PatchMaster software (HEKA). The recording pipettes had resistances of 0.3–1 MΩ, when filled with 2M KCl. The extracellular medium contained (mM) 115 NaCl, 2.5 KCl, 1.8 $CaCl_2$, and 10 HEPES, pH 7.2/NaOH. In some experiments, 5 mM $MgCl_2$ was added to the extracellular solution. For measurement of tail currents or constitutively active channels, K^+ concentration was elevated to 60 mM, replacing Na^+. In the case of channels that had no constitutive activity, P/4 or P/8 protocol was used to subtract leak and capacitance currents from a holding potential of −100 or −120 mV.

Voltage-clamp fluorometry (VCF)

To reduce unspecific labeling of endogenous cysteines on the surface, the oocytes were incubated for 30 min at room temperature with 0.1–0.5 mM glycine maleimide, following 3–4 d at 12°C, during which time the channel protein was made but not transported to the plasma membrane. Subsequently, the oocytes were washed extensively with ND-96 and left overnight at room temperature to allow the nascent channels to come to the plasma membrane. On the next day, they were labeled for 1 h on ice in darkness with 12.5 µM tetramethylrhodamine maleimide (TMRM; Invitrogen) diluted in depolarizing solution (mM: 92 KCl, 1.8 $CaCl_2$, and 10

Published March 30, 2017

HEPES, pH 7.5/NaOH). After labeling, the oocytes were washed extensively with ND-96 and kept at 16°C in darkness until recording. VCF signals were recorded through 20× 0.75-NA fluorescence objective (Nikon). The illumination source was a 150-W xenon lamp. The light path contained HQ535/50 excitation filter, HQ610/75 emission filter, and Q565LP dichroic mirror (Chroma Technology). The emitted light was collected with an HC120-05 photomultiplier tube (Hamamatsu). During fluorescence recordings, the oocytes were voltage clamped using a Dagan CA1-B amplifier. Fluorescence and current signals were low-pass filtered at 1 kHz, digitized at 5 kHz with a Digidata-1440A analogue-to-digital converter (Axon Instruments), and acquired with pCLAMP10 software (Axon Instruments). To increase signal to noise ratio, each VCF trace was averaged 10 times.

MTS accessibility assay

[2-(trimethylammonium)ethyl]methanethiosulfonate bromide (MTSET) was purchased from Toronto Research Chemicals. 100 mM stock solutions (in water) were kept at −80°C, thawed on ice, and diluted in the extracellular solutions to a final concentration of 200 µM immediately before each recording. The oocytes were voltage clamped, as described in the section Electrophysiological recordings. GV shifts upon MTS ET application were assessed by running the GV protocol before and after 1-min exposure to MTSET at 0 or −100 mV. Increase in current as a function of time with MTSET was monitored by repetitive pulsing to −40 mV (full-length channel), −120 mV (L341 split, MTSET exposure at 0 mV) and −160 mV (L341 split, MTSET exposure at −100 mV). These voltage steps were selected based on large changes of GV curves before and after MTSET application. To avoid clamping the constitutively active L341 split at voltages far from K^+ equilibrium potential, we used extracellular solution containing 2.5 mM K^+ for the hyperpolarized protocol or 60 mM K^+ for the depolarized protocol.

Single-molecule colocalization

Single-molecule imaging was performed 24–48 h after RNA injection using total internal reflection fluorescence (TIRF) microscopy. Manually devitellinized oocytes were placed on high-refractive-index coverglass (n = 1.78) and imaged through a 100× 1.65-NA oil immersion objective (Olympus). 13 × 13–µm frames showing low density (50–250 individual puncta per frame) to minimize the risk of false colocalization were imaged. EGFP-tagged VSDs and full-length subunits were excited with a PhoxX 488 (60 mW) laser, and mCherry-tagged PDs and full-length subunits were excited with a 593-nm diode-pumped solid-state (DPSS) laser. z488/594-rpc polychroic (Chroma) was used as the excitation filter; 525/50 and 629/53 emission filters were used for EGFP and mCherry, respectively. mCherry and EGFP were excited sequentially. Videos of 800 frames (~200 for mCherry and 600 for EGFP) were captured at the rate of 20 Hz with the iXon DU-887 EMCCD camera (Andor Technology).

The bleaching videos of the PD tagged with EGFP were acquired in a similar way, using Nikon 100× 1.49 NA oil immersion TIRF objective. Devitellinized oocytes were placed on 35-mm µ-dishes with glass bottom (n = 1.52; IBIDI). They were excited with a 488-nm laser. The light path contained a 525/50-nm emission filter. The videos were captured with iXon DU-897 EMCCD camera (Andor Technology) at 10 Hz.

Data analysis and statistics

In each experiment, we used oocytes isolated from at least two different frogs. The sample numbers are indicated in the figure legends. For statistical analysis, we used Student's t test if two groups were compared or analysis of variance followed by multiple comparisons with Bonferroni's correction if more groups were compared. Electrophysiological recordings were analyzed with IGOR Pro (WaveMetrics) or Fitmaster (HEKA). Conductance and current deactivation kinetics were obtained from biexponential fits to tail currents: $I(t) = A_1 * \exp(-t/\tau_1) + A_2 * \exp(-t/\tau_2) + I_0$, where I is the current, t is the time, τ_1 and τ_2 are the time constants of the fast and the slow component, A_1 and A_2 are the corresponding amplitudes, and I_0 is the offset current. The conductance is proportional to $I(t = 0)$. However, in the case of constitutively active split channels, a capacitance transient often contaminated tail currents, because P/n leak subtraction was not possible. Conductance was then calculated as the ratio of the steady-state current and the driving force: $G = I/(V - V_K)$, where G is the conductance, I is the steady-state current, V is the voltage, and V_K is the equilibrium potential for K^+. Because the constitutively active channels showed large inward currents, V_K could be estimated from the zero crossing of the current-voltage curve for each oocyte (assuming that the influence of other conductances on the current-voltage curve is negligible). Conductance values were normalized to the maximum, averaged, and fitted with the following Boltzmann function: $G/G_{max} = 1/(1 + \exp(-k * (V - V_{1/2})))$, where G/G_{max} is the normalized conductance, k is the slope factor, V is the voltage, and $V_{1/2}$ is the voltage for which the conductance is half maximal. Current activation kinetics were compared by quantifying the time needed for current to reach 90% of its maximal value.

VCF recordings were analyzed with Clampfit (Axon Instruments) and IGOR Pro. To measure kinetics, activation and deactivation phases of the fluorescence traces were fitted with single-exponential functions. Baseline-subtracted, steady-state changes of fluorescence as a function of voltage were normalized to the

Published March 30, 2017

maximal value, averaged between oocytes expressing the same channel, and fitted with a Boltzmann function equivalent to the one used for conductance.

Changes in current upon MTSET application were normalized as $-(I_t - I_0)/(I_{max} - I_0)$, where I_t is the peak current at time point t, I_0 is the mean peak current evoked in the absence of MTSET, and I_{max} is the peak current upon completion of the MTSET modification. To obtain MTSET modification time constants (τ_{MTSET}), current amplitude was plotted for each cell against the time with MTSET and fitted with a single exponential function. The modification rate constants were then calculated as $1/(\tau_{MTSET} * [MTSET])$, assuming pseudo-first-order reaction.

Colocalization between EGFP and mCherry puncta was analyzed manually. The first three to five frames of the bleaching videos were averaged for each channel, and the relative localization of EGFP and mCherry spots was determined (two spots were considered colocalized if they were within 3 pixels from one another, which corresponds to 150 nm). Only single, stable spots were included in the analysis. Colocalization coefficients presented in the Results section are defined as the number of overlapping spots divided by the sum of overlapping and nonoverlapping spots. We used the following equation to subtract density-dependent, random colocalization: $f = a * dg * dr/(dg + dr)$, where f is the random colocalization, a is the area of a diffraction-limited spot with a radius of 150 nm, dg is the density of green puncta, and dr is the density of red puncta.

Online supplemental material

Figs. S1–S11 describe control and validation experiments and aspects of the characterization of some mutants that were omitted in the main text for clarity. Videos 1–4 show examples of single-molecule bleaching experiments.

RESULTS

Constitutive activity of channels with interrupted S4 helix

In light of our previous finding of functional voltage-gated $K_V10.1$ channels that lack a covalent bond between VSD and PD (Lörinczi et al., 2015), we asked whether disrupting the channel in different positions gives various outcomes or it uniformly leads to split channels that resemble the wild type. To answer this question, we generated a series of split channels, removing the covalent bond after every residue from K340 to A349 (Fig. 1 A). Each of the split channels was heterologously expressed in *Xenopus* oocytes and characterized with two-electrode voltage clamp. Strikingly, interrupting the channel within the S4 (after residues K340, L341, D342, and H343) resulted in channels that were constitutively active, as indicated by inward currents at negative potentials. When the break was made in the S4–S5 linker or at the bottom of S5, constitutive activity was greatly reduced (after residues Y344 and I345) or completely absent (after residues E346, Y347, G348, and A349; Fig. 1 C). Both outward and inward currents through channels that had constitutive activity could be blocked by the $K_V10.1$ blocker astemizole (Fig. S1). Furthermore, no current distinguishable from the control group was recorded when G440S mutation was introduced in the selectivity filter of these channels, which renders them nonconducting, confirming that their constitutive activity is not caused by flux of ions through the gating pore in the VSD (Tombola et al., 2005). Interestingly, we also noticed that the split channels, which did fully close except for Y347 split, had the conductance-voltage (GV) curve shifted to more positive values or showed a biphasic dependency of open probability on voltage with a nonsaturating component (Fig. S2), suggesting that the importance of the covalent connection between the VSD and the PD is not limited to the transition into a stable resting state. Collectively, our results reveal that breaks within S4 result in constitutively active split channels, but interruptions of the S4–S5 linker do not.

Disconnection between the S4–S5 loop and the S5 helix dramatically alters channel kinetics

The channels split after Y347 and G348 showed radical alterations of channel kinetics. Although Y347 split could eventually close completely, deactivation took up to 20 s, whereas it did not exceed 300 ms in the wild-type channel (Fig. 2 A). Remarkably, the fast deactivation time constant nearly overlapped between the continuous channel, Y347 split and G348 split (Fig. S3, A and B), but Y347 split had an additional super slow component with some voltage dependency, as complete closure was faster at more negative potentials. G348 split also showed slower deactivation, but the effect was smaller than in Y347 split.

The activation kinetics of $K_V10.1$ strongly depends on the membrane potential before the stimulus (Ludwig et al., 1994), probably reflecting voltage-dependent transitions between different closed states. To study the kinetics of entry into deeper closed states, we used a reactivation protocol, in which channels were opened with a pulse to 40 mV, then stepped to −120 mV for a variable time and opened again with another pulse to 40 mV. As more channels populate deeper closed states, current activation is delayed in proportion to the interval at negative potential. Even though some channels remained open at the end of the negative segment of the pulse (because of the super slow deactivation), Y347 split activated slower at every time interval compared with the wild type (Fig. 2 B). The slowing down of activation of G348 split was yet more pronounced, and all the rise times were an order of magnitude slower than

Published March 30, 2017

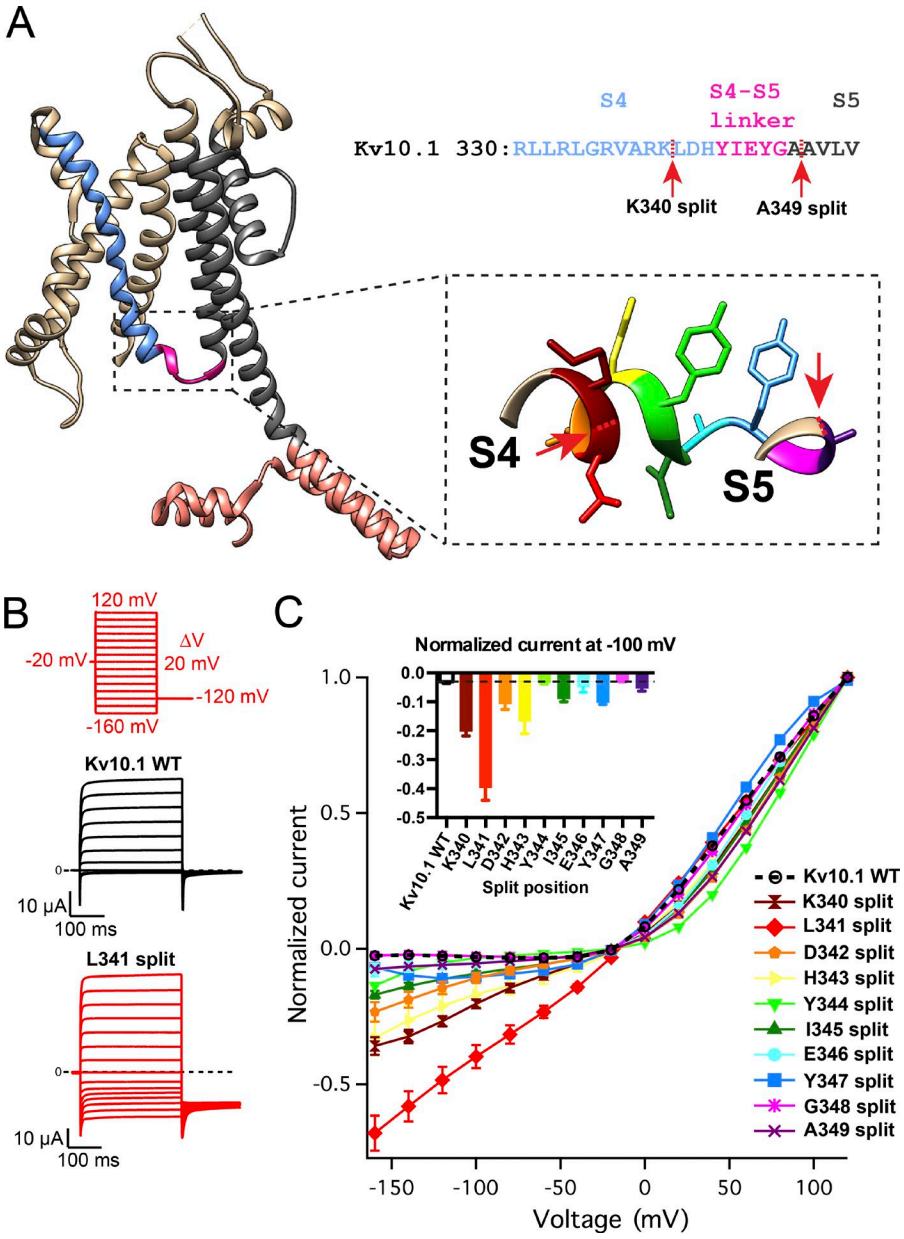

Figure 1. **Constitutive activity of channels split within S4.** (A) Lateral view of a K_V10.1 subunit (PDB code 5K7L). The S4 helix is indicated in light blue, the S4–S5 linker in pink, the PD helices in gray, and the C linker in salmon. (Top right) K_V10.1 sequence in the S4 helix and in the S4–S5 linker. We generated a series of split channels by disconnecting the VSD from the PD after every residue between the positions shown by red arrows. (Inset) The C-terminal S4 helix and the S4–S5 linker colored in a way corresponding with data points in C. (B) Representative, macroscopic currents of the wild-type channel and L341 split recorded without leak subtraction. (C) Normalized, mean current-voltage curves of the wild-type and several split channels (n = 6–14). Error bars denote SEM. (Inset) Normalized current at −100 mV plotted against the split position (mean ± SEM); dashed line shows the current level in the wild type.

in the wild type. Moreover, at voltages slightly above their activation threshold, both split channels were in a profoundly slower kinetic regimen compared with the wild type (Fig. S3, C and D).

We then asked whether the altered kinetics of Y347 split, which showed major changes in both activation and deactivation, could be explained by changes in VSD motion. To test this, we introduced the mutation I319C, which reports on voltage-sensing motions in K_V10.1 when labeled with TMRM (Schönherr et al., 2002). We quantified the kinetics of the VCF signal elicited by a voltage step from −100 to 60 mV (Fig. 2 D). The activation time constant was significantly faster in the full-length channel than in Y347 split (3.0 ± 1.5 ms and 15.1 ± 2.4 ms; mean ± SD, $P < 1 \times 10^{-6}$, t test), whereas the deactivation time constant was similar in both cases (19.3 ± 6.4 ms and 18.2 ± 1.4 ms, respectively; Fig. 2 E). Thus, the slower current activation in Y347 split can be partly attributed to slower VSD movement, but the super slow deactivation component remains unexplained.

Restoration of channel closure by point mutations

Disconnection between VSD and PD could change biophysical properties of the channel because of a gross structural change. Alternatively, precise functional interactions of residues in the S4–S5 linker region with their counterparts at the channel gate or in the cytoplasmic domains could be disturbed. If a change affecting large regions of the channel protein is involved, it is unlikely that wild type–like properties could be restored by point mutations. To test this, we

Published March 30, 2017

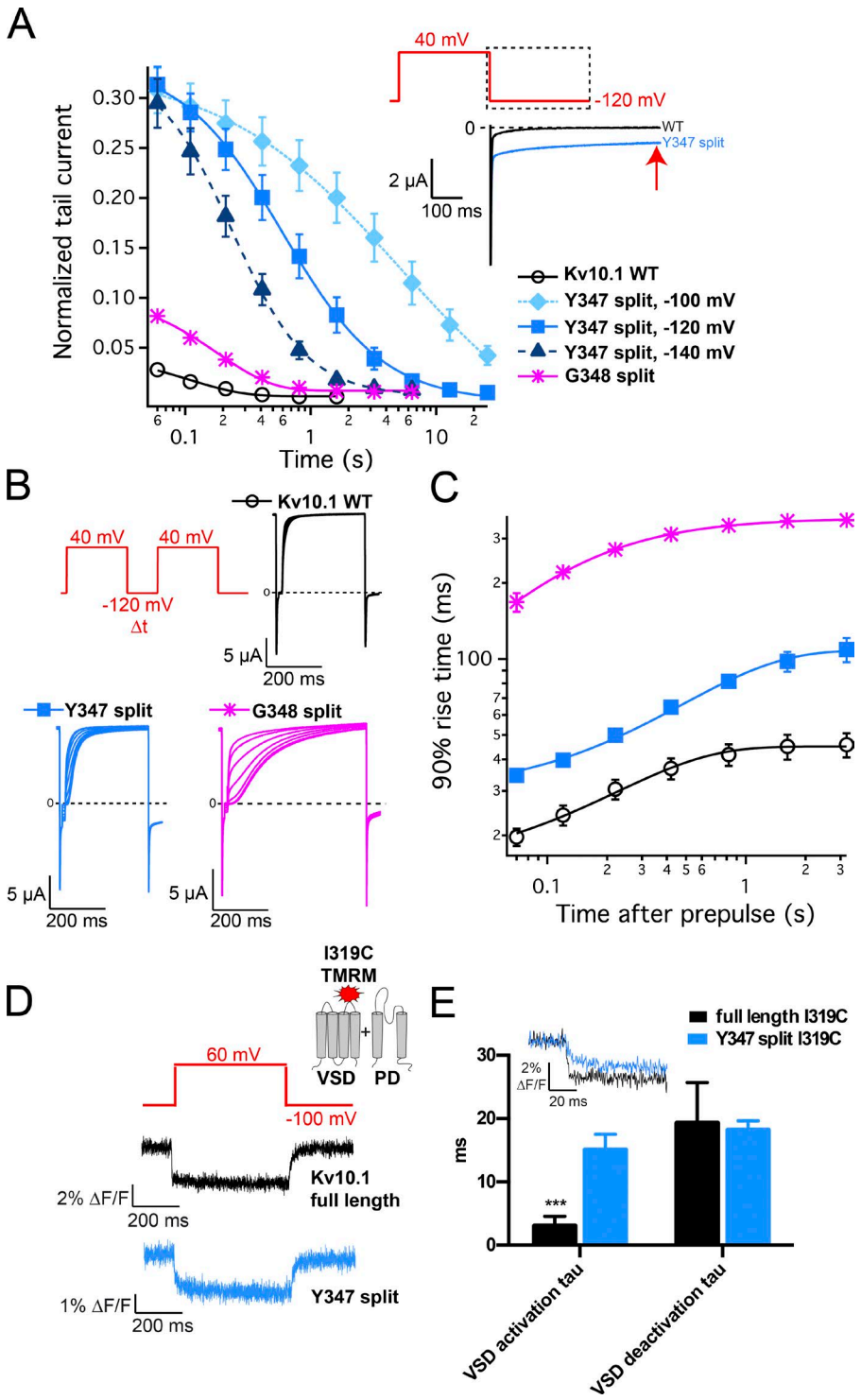

Figure 2. **Alterations of channel kinetics in Y347 split and G348 split.** (A) Tail current, normalized to the steady-state current at the end of the depolarizing segment of the voltage pulse, plotted against time at negative potential (mean ± SEM; *n* = 6). (Top right) Super slow deactivation component indicated by the red arrow. (B) Representative currents of the wild type, Y347 split, and G348 split recorded with the reactivation protocol with various intervals at −120 mV between the depolarizing pulses. (C) Time needed for current to reach 90% of its maximal value plotted against the length of the interval at −120 mV (mean ± SEM; *n* = 6–8). (D) Representative voltage-dependent changes of fluorescence reported by I319C-TMRM, elicited by a depolarization to 60 mV from a holding potential of −100 mV. (E) Activation and deactivation time constants obtained by exponential fits to fluorescence traces (*n* = 5–8; mean ± SD). Asterisks indicate statistical significance ($P < 0.001$). (Inset) Superimposed VCF traces from D with an expanded time base.

first turned to mutagenesis of D342 because the homologous D540 plays an important role in channel closure of the closely related $K_V11.1$ and interacts electrostatically with R665 (homologous to Q477 in $K_V10.1$) at the channel gate at negative potentials (Tristani-Firouzi et al., 2002; Ferrer et al., 2006).

Constitutive activity of L341 split was assessed after mutating D342 to 12 amino acids with different physicochemical properties. Strikingly, all of them, except for N, which is isosteric with the wild-type residue (D), greatly facilitated closure, irrespectively of side chain size, charge, and hydrophobicity (Fig. 3 and Fig. S4 A). At −100 mV, only the two mutated split channels with N and L at position 342 had significantly more current than the wild type (Bonferroni's multiple comparisons test). However, at −160 mV, nearly all the mutants had

Published March 30, 2017

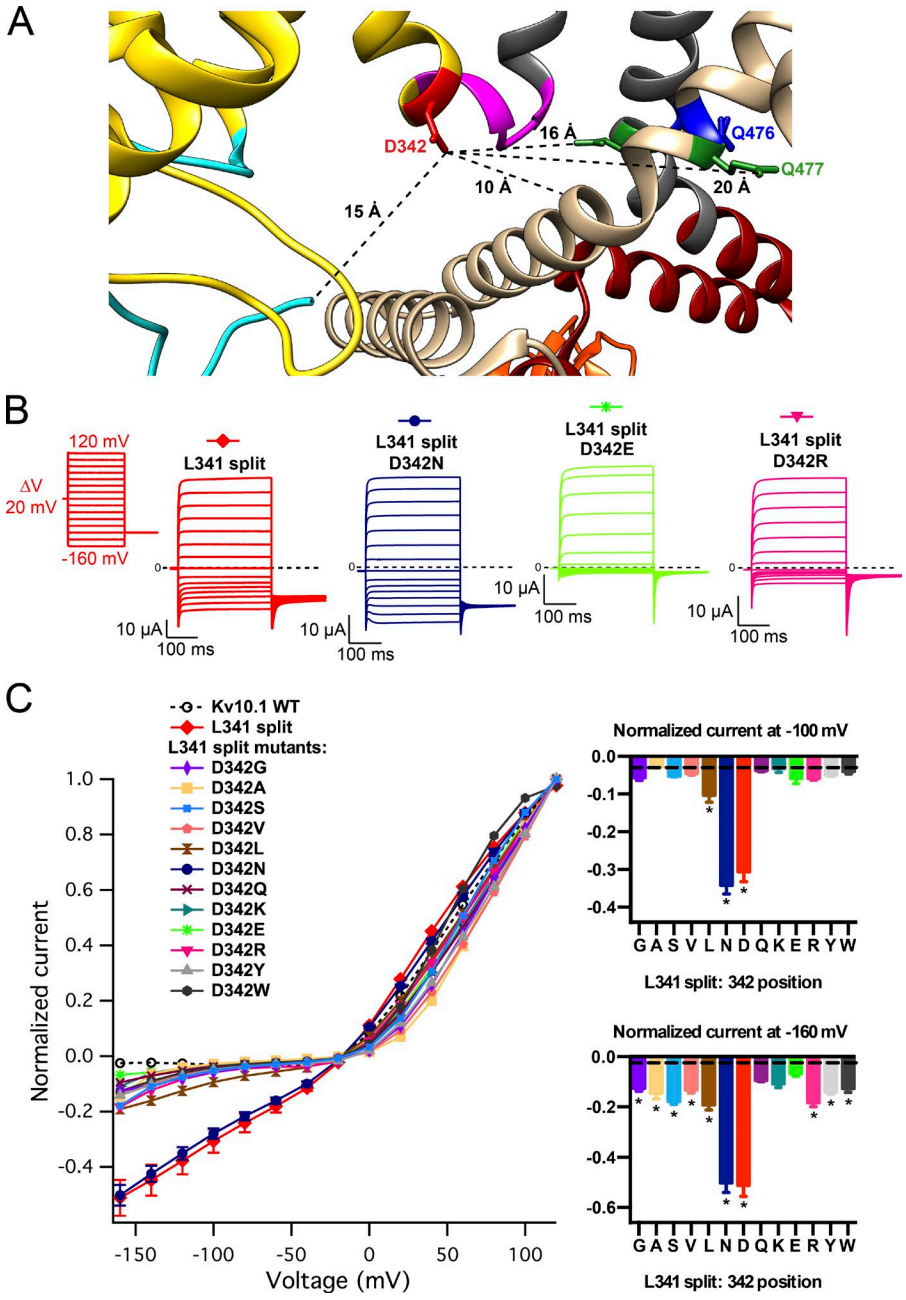

Figure 3. **Restoration of wild type–like closure with point mutations of D342.** (A) The position of D342 in the activated VSD. For clarity, only two subunits are shown, and one of them is color coded: the N-terminal PAS domain is shown in cyan, the VSD in yellow, the S4–S5 linker in magenta, the PD helices in gray, the C linker in dark red, and the CNBHD in orange. The crucial residues are color coded in both subunits: D342 in red, Q476 (S6 bundle crossing) in blue, and Q477 in green. (B) Representative currents of L341 split and selected D342 mutants in L341 split. The voltage protocol is shown at the top. (C) Normalized, mean current values plotted against voltage (n = 7–18). Error bars denote SEM. Insets contain normalized current at −100 and −160 mV plotted against the residue at 342 position (mean ± SEM). The order from left to right reflects residue size, and dashed lines indicate the current level of the wild type. Asterisks indicate statistical significance ($P < 0.05$ in t test with Bonferroni correction) with respect to the continuous channel.

significantly more current than the wild type, suggesting that they might reopen at very hyperpolarized voltages. Except for W, the corresponding D342 mutants in the full-length channel produced a rightward shift of the GV curve, suggesting that D342 participates in an interaction that favors the open state (Fig. S5). Interestingly, D342W mutation resulted in channels that were permanently open, which would be compatible with a steric hindrance between the bulky W residue and the channel gate at negative voltages. However, this effect did not occur in the split channel, suggesting that the position of this residue might change when VSD and PD are not covalently bound. Also, a deletion of D342 or longer deletions starting from D342 restored channel closure in the background of L341 split (Fig. S4, B and C). Particularly interesting is the Δ342–348 split, which is missing both the C-terminal S4 and the S4–S5 linker loop and yet can close completely.

We next checked whether the aromaticity of Y347 is relevant for the disruption of channel kinetics seen in Y347 split. Mutations to F and L eliminated the super slow deactivation component and enabled complete closure within 500 ms (Fig. S6, A and B). Notably, Y347F and Y347L mutants also had slower activation kinetics and biphasic GV curves (Fig. S6, C and D). Because F did not mimic Y, whereas the effects of F and L mutations were almost indistinguishable, the aromatic ring at position 347 does not seem responsible for the

Published March 30, 2017

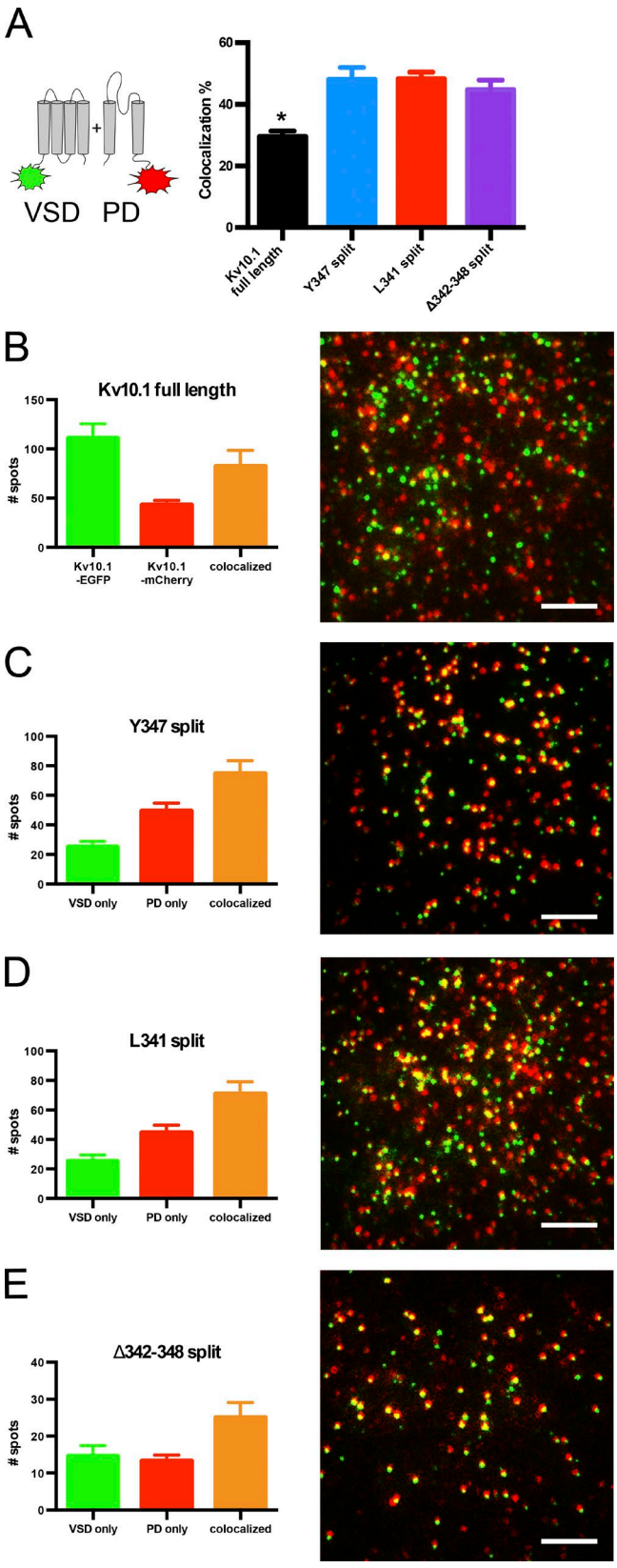

Figure 4. **Single-molecule colocalization between fluorescently tagged VSD and PD.** (A) Mean colocalization coefficients ± SEM, after subtraction of random colocalization (n = 8–14); asterisk indicates statistical significance ($P < 0.05$ in t test with Bonferroni correction) with respect to the wild-type channel. Tagged full-length subunits were used as positive control. (B–E) Representative 13 × 13–µm images for each condition and mean numbers of fluorescent spots per image ± SEM. Bars, 2.5 µm.

changes of kinetics in the split channel. This result points to the importance of the tyrosine hydroxyl group, which is the only structural difference between Y and F, making Y slightly less hydrophobic and allowing it to participate in hydrogen bonds. Besides, having a large hydrophobic residue at this position might be important, as mutations to A and S considerably reduced functional expression.

These findings suggest that even if the C-terminal S4 and the S4–S5 linker are not continuous, their residues maintain important functional interactions between VSD and PD. Furthermore, it is truly striking that C-terminal S4 can be truncated and disconnected from the S4–S5 linker and the PD with relative impunity if D342 is deleted or mutated. This could mean that the novel gating mechanism in K_V10.1 is not restricted to the interaction between the C-terminal S4 and the C linker at negative potentials.

Single-molecule colocalization between fluorescently tagged VSD and PD

Changes in the biophysical properties might arise from differences in the assembly of split channels. To analyze the coassembly between VSD and PD, we used the method of single-molecule subunit counting/colocalization (Ulbrich and Isacoff, 2007), where fluorescently tagged channels were transiently expressed in *Xenopus* oocytes. Oocytes provide a convenient experimental system for controlled protein expression at a level where well-separated fluorescent spots are observed (Fig. 4). We tagged VSD with EGFP at the N terminus and PD with mCherry at the C terminus and determined their relative localization in the plasma membrane using TIRF microscopy (see Materials and methods).

Upon expression of mCherry-tagged PD only, we found stable diffraction-limited spots when the oocytes were excited with 593-nm laser light (Video 1). EGFP-tagged VSD either did not appear in the plasma membrane or only few very mobile spots were detected on the surface of the oocytes excited by a 488-nm laser (Video 2). In contrast, when EGFP-tagged VSD was expressed in presence of mCherry-tagged PD, we found very stable spots for both PD and VSD, indicating that expression of VSD requires the presence of PD or that PD stabilizes the expression of VSD in the plasma membrane (Video 3).

Because the efficient surface expression of VSD required the expression of PD, we expected higher colocalization between the two than when full-length

Published March 30, 2017

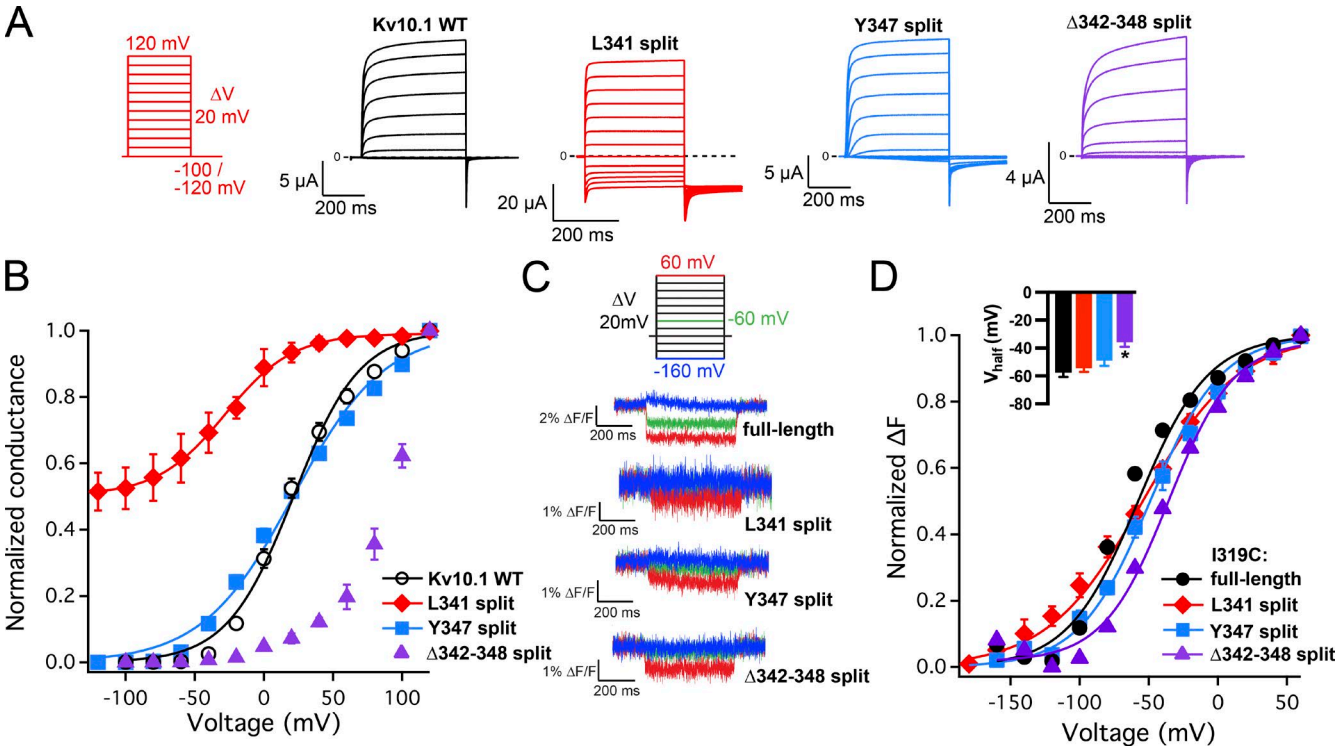

Figure 5. **Voltage dependency of conductance and VSD activation in specific split channels.** (A) Representative currents of the wild-type, L341 split, Y347 split, and Δ342–348 split recorded with the indicated voltage protocol, with the exception of L341 split where the holding potential was −20 mV. (B) Normalized conductance plotted against voltage (mean ± SEM; n = 7–10). The curves are Boltzmann fits with the following $V_{1/2}$ values (mean ± SD): −28.0 ± 1.8 mV (L341 split), 21.4 ± 1.7 mV (WT), and 21.7 ± 2.1 mV (Y347 split). Fitting was not done for the Δ342–348 split because the conductance did not saturate in the voltage range tested. (C) Representative voltage-dependent fluorescence changes reported by I319C-TMRM. Only traces elicited by the voltage steps of −160 (blue), −60 (green), and 60 (red) mV are shown. (D) Normalized fluorescence changes plotted against voltage (mean ± SEM; n = 5–10); asterisk indicates statistical significance ($P < 0.05$ in t test with Bonferroni correction) with respect to the continuous channel. The curves are Boltzmann fits. Inset contains $V_{1/2}$ values of the Boltzmann fits (mean ± SD): −54.3 ± 2.8 mV (L341 split), −57.7 ± 3.0 mV (WT), −49.0 ± 3.6 mV (Y347 split), and 35.6 ± 3.4 mV (Δ342–348 split).

subunits, which are either EGFP or mCherry tagged, are expressed together (EGFP- and mCherry-tagged full-length subunits can form homotetramers—EGFP- or mCherry-only spots—thereby reducing the colocalization coefficient). In the case of full-length subunits, we observed many more non-colocalized EGFP than mCherry puncta, probably owing to more efficient maturation of EGFP (Padilla-Parra et al., 2009; Macdonald et al., 2012).

We selected three split channels with very different biophysical properties, L341 split, Y347 split, and Δ342–348 split, and confirmed that their tagged versions are functional (Fig. S7). Interestingly, the N-terminal EGFP fusion greatly reduced the constitutive activity of L341 split. We imaged six to eight oocytes from three different batches and analyzed 50–250 fluorescent spots per patch in 8–14 optical patches. After subtraction of random colocalization (see Materials and methods), we got a very similar colocalization coefficient for all three split channels tested (48 ± 2%, 48 ± 4%, and 45 ± 3%, respectively; mean ± SEM; Fig. 4 A), significantly higher compared with the full-length subunits (30 ± 2%). We also noted that few green-only (EGFP) spots were visible when VSD and PD were not covalently bound, in spite of the more efficient maturation of EGFP, indicating again that the presence of PD stabilizes the surface expression of VSD (Fig. 4, C–E). We did observe a few non-colocalized VSDs, but they could coassemble with nonfluorescent PDs (based on previous experience, we estimate the maturation efficiency of mCherry fusion constructs at 50%).

Collectively, these results suggest that the VSD requires the PD to be present in the membrane, when they are not covalently bound. On the contrary, the PD is able to go to the membrane alone. Also, interrupting the channel in different position does not seem to affect VSD-PD assembly.

Breaks in the S4–S5 linker affect VSD movement and coupling with PD

We next asked whether interrupting the C-terminal S4 helix or the S4–S5 linker affects the voltage dependency of VSD motion. For instance, the failure of the constitutively active split channels to close completely at nega-

Published March 30, 2017

tive potentials might be caused by a bias toward the activated conformation of the VSD. To test this hypothesis, we measured the voltage dependency of VSD activation by VCF. We used I319C mutants labeled with TMRM, after verifying that I319C mutation by itself has only limited consequences for the voltage dependency of the channel (Fig. S8). As in the colocalization experiments, we focused on three split channels that cover the whole spectrum of GV curves: left-shifted and constitutively active L341 split, right-shifted Δ342–348 split, and Y347 split with no significant shift compared with the wild type (Fig. 5, A and B).

Although the absolute magnitude of VCF signals is not directly comparable because the photomultiplier gain was adjusted individually for every oocyte, we noted that split constructs showed smaller voltage-dependent changes of fluorescence than the full-length channel, probably owing to a difference in expression levels. Among the split channels, L341 split consistently gave the lowest signal (Fig. 5 C). Surprisingly, the midpoint of fluorescence-voltage (FV) curves was nearly overlapping between the full-length channel (−57.7 ± 3.0 mV; mean ± SD) and L341 split (−54.3 ± 2.8 mV; Fig. 5 D). In contrast, Y347 split and Δ342–348 split showed modest positive FV shifts (midpoint at 49.0 ± 3.6 mV and 35.6 ± 3.4 mV, respectively). Interestingly, the separation of GV and FV curves decreased in Y347 split and increased in Δ342–348 split, with respect to the full-length channel (a rigorous estimation was impossible for Δ342–348 split because the GV curve did not reach plateau in the voltage range tested).

We next looked for additional evidence that L342 split remains open despite full VSD deactivation. Because VCF only reports local protein motions around the fluorophore, it is also possible that in L341 split the VSD as a whole is not allowed to reach the same resting conformation as in the full-length channel. To test this, we checked whether the activation kinetics of L341 split are slowed down by Mg^{2+}, an allosteric stabilizer of the closed conformation which binds to the VSD (Silverman et al., 2000). We used a protocol with a depolarizing step to 40 mV after a 5-s prepulse to different voltages in the presence or absence of 5 mM Mg^{2+}. In the full-length channel, Mg^{2+} slowed down activation at all conditioning potentials (Fig. 6). Strikingly, Mg^{2+} had almost no effect on L341 split. This could reflect a difference in the accessibility or affinity of the Mg^{2+}-binding site caused by a different resting position of the VSD. Alternatively, it is possible that Mg^{2+} binding has little or no effect because VSD and PD are decoupled. We also assessed Mg^{2+} effect in the other split channels. Surprisingly, the slowing down of activation kinetics was greatly augmented in Y347 split compared with the full-length channel (Fig. 6 B). The activation kinetics of Δ342–348 split were unaffected by Mg^{2+}, but we observed significant increases of the peak current for the most hyperpolarizing prepulses with Mg^{2+} ($P < 0.0001$ for −160 and −140 mV, $P < 0.001$ for −120 mV, Bonferroni's multiple comparisons test; Fig. 6 C).

To probe the VSD conformational changes in L341 split further, we did an accessibility assay to membrane-impermeable MTS reagents. Conjugation of MTS reagents to cysteine residues substituted at meaningful positions in the channel changes the current. The modification rate is assumed to be proportional to their solvent accessibility, which might be influenced by voltage-dependent conformational changes. We expected that if the resting position of the VSD is different between the full-length channel and L341 split, we would observe changes in accessibility of cysteine residues substituted in the upper S4 helix. We focused on I319C and L322C mutants, which show a negative GV shift upon application of 200 µM MTSET (Fig. S9). We assessed the voltage dependency of their accessibility, using two protocols with holding potentials of 0 and 100 mV.

The modification rates were very close between the full-length channel and L341 split for both the weakly voltage-dependent I319C site and the strongly voltage-dependent L322C site, suggesting that the S4 helix undergoes similar conformational changes (Fig. 7, C and D). Interestingly, the change in current induced by MTSET application was almost overlapping between the full-length channel exposed at 0 mV and L341 split exposed at both 0 and −100 mV and more than twofold larger for the full-length channel exposed at −100 mV (Fig. 7, A and B). This indicates that the transition from the closed to the open state is most affected by MTS conjugation because the increase of current is reduced if a large fraction of channels is open during MTS application, as it is the case for all tested conditions, except for the full-length channel at −100 mV. Collectively, these results suggest that interrupting the channel in the C-terminal S4 or in the S4–S5 linker has surprisingly little or no influence on the voltage dependency of S4 motion. If this holds true, split channels provide an excellent model to study coupling between VSD and PD because the voltage-dependent conformational changes of the VSD seem to be very similar to the WT channel and yet produce radically different gating outcomes.

PDs carrying mutations that lock the full-length channel in the active state fail to give rise to currents when expressed alone

The constitutive activity of L341 split could result from weaker coupling, if the pore intrinsically preferred the open conformation and conformational changes in the VSD were not efficiently transmitted to it. Alternatively, if the pore had an intrinsic preference for the closed conformation, as proposed for other K_V channels (Yifrach and MacKinnon, 2002; Pless et al., 2013), constitutive activity could result from an increase in

Published March 30, 2017

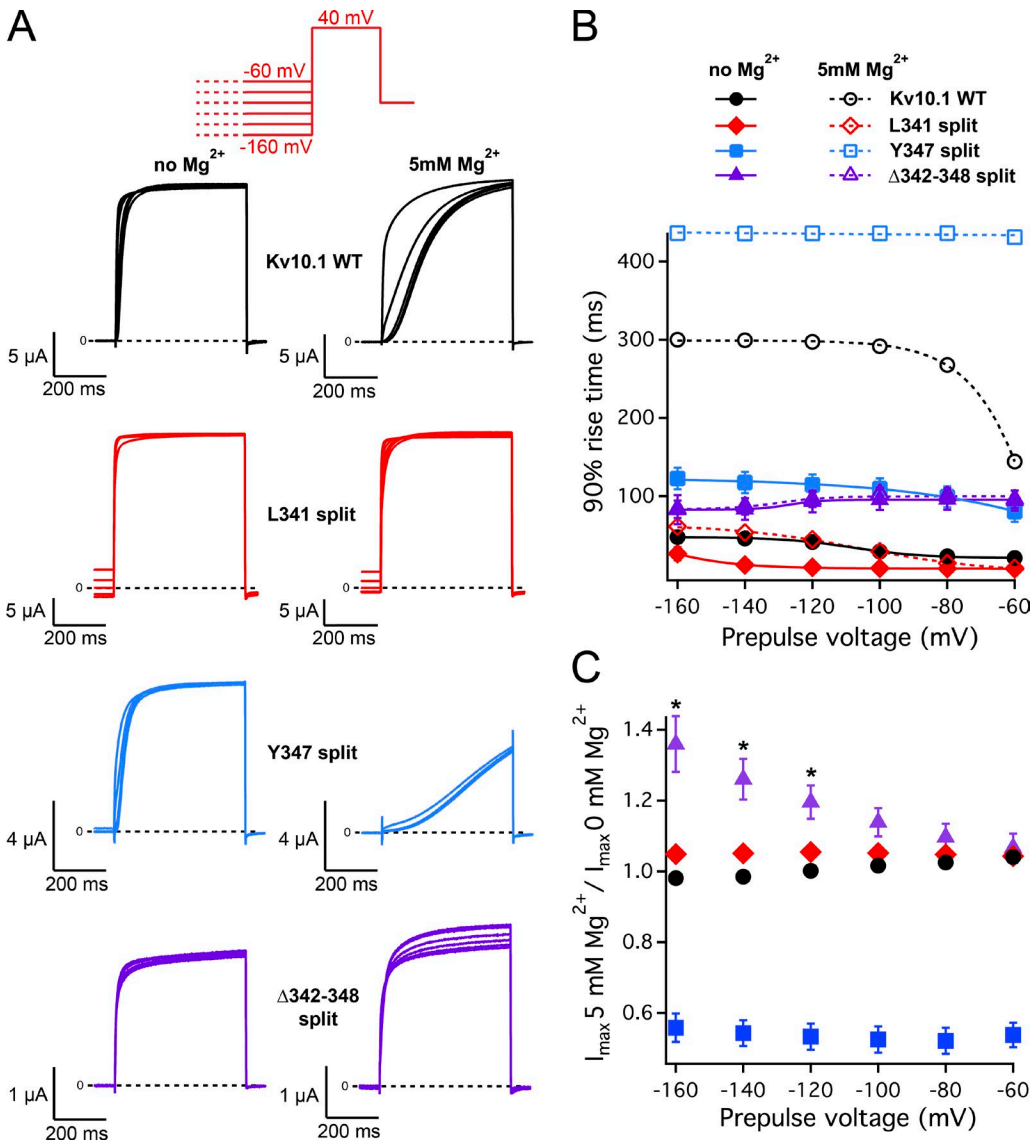

Figure 6. **Effects of prepulse voltage Mg^{2+} on activation kinetics of specific split channels.** (A) Representative currents of the wild type, L341 split, Y347 split, and Δ342–348 split elicited with the indicated voltage protocol, with (left) and without (right) 5 mM Mg^{2+} in the extracellular medium. In the voltage protocol, the duration of the conditioning prepulse was 5 s. (B) Time needed for current to reach 90% of the maximal value plotted against the prepulse voltage (mean ± SEM; n = 7–10). (C) The ratio of peak currents with and without Mg^{2+} in the extracellular medium (mean ± SEM; n = 7–10; asterisks indicate $P < 0.05$ in t test with Bonferroni correction with respect to the continuous channel).

the coupling strength that would strongly bias the channel toward the open state. To distinguish between these options, we decided to probe the PD expressed in isolation. We took advantage of the fact that the S6 helix of KCNH channels lacks the PVP hinge, which acts as a pivot important for gating in Shaker family channels (Long et al., 2005b, 2007). Following a study in $K_V11.1$ (Thouta et al., 2014), we speculated that introducing a proline at certain positions in S6 would lock the channel in the open state by forcing a break in S6 helix. Indeed, we found that mutating Q476 and Q477 to P results in constitutively active full-length channels with large currents (Fig. 8, A and B). Interestingly, Q476P mutation caused a strong inward rectification, whereas Q477P mutant had a nearly linear dependence of current on voltage. The cryo-EM structure of $K_V10.1$ revealed that these residues are localized at the S6 helix bundle crossing (the side chains of Q476 occlude the permeation pathway in the closed conformation of the channel, whereas Q477 is facing outward, toward the VSD).

Given our observation of PD complexes without VSD at the single-molecule level, we next checked whether proline substitutions in S6 have a similar effect on PD expressed alone. Q476P mutation failed to give rise to K^+ currents when the PD was expressed alone or to-

Published March 30, 2017

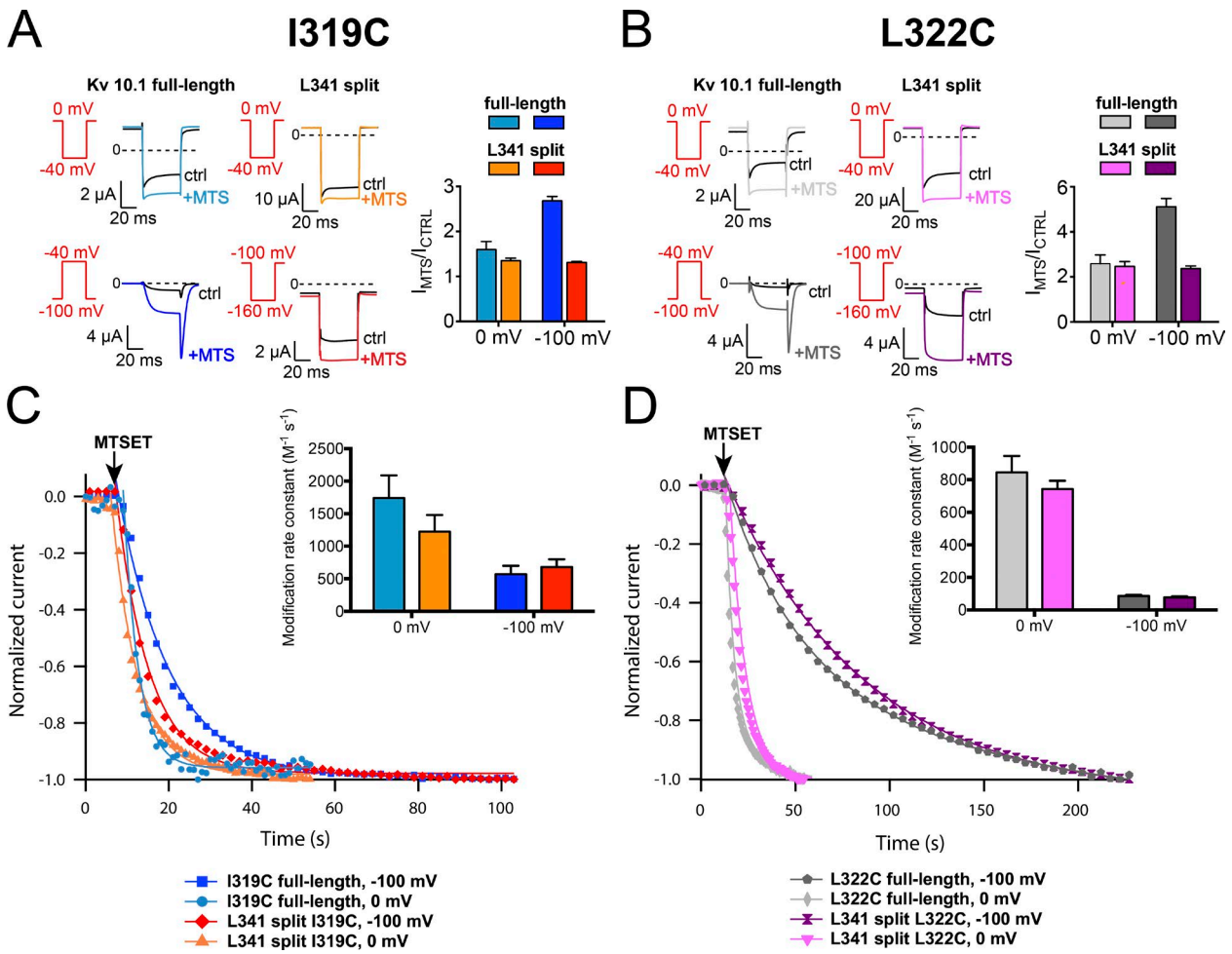

Figure 7. **Voltage dependence of accessibility to MTSET overlaps between the full-length channel and L341 split.** (A and B) Representative currents and mean current ratios (±SEM) from I319C (A) and L322C (B) mutants before and after application of 200 µM MTSET at 0 or −100 mV. (C and D) Representative graphs showing the time course of current changes upon MTSET application at hyperpolarized and depolarized potentials for the weakly voltage-dependent I319C site (C) and the strongly voltage-dependent L322C site (D). Curves represent single-exponential fits to data points from individual cells. Insets contain histograms with mean modification rate constants ± SEM (n = 5–8).

gether with the VSD (Fig. S10). Q477P mutant was also nonconducting in the isolated PD, but upon coexpression with VSD the resulting split channel was constitutively active (Fig. 8, C and D). Unexpectedly, it showed strong rectification, with the conductance decreasing at positive potentials, similarly to Q476P mutation in the full-length channel. We also verified that EGFP-tagged PD with Q477P mutation is transported to the membrane when it is expressed without the VSD (Video 4). These findings suggest that the isolated pore has a thermodynamic preference for a nonconducting conformation. Moreover, even if access to the pore is granted by a proline break in S6, the presence of VSD is still necessary for permeation, in contrast to the results obtained with sensor-less pores of specific bacterial channels that adopted the open conformation without the VSD (Santos et al., 2008; McCusker et al., 2011, 2012; Shaya et al., 2011; Syeda et al., 2012). To investigate this idea further, we introduced mutations in the VSD that shift the voltage dependency of the channel to positive (R333Q) and negative values (R336Q; Fig. S11). Remarkably, the additional VSD mutations did not make a difference in the background of Q477P mutation in PD, as the resulting split channels behaved almost equally (Fig. 8, E and F). Their dependence of conductance on voltage is best fit by a parabola, possibly owing to some degree of intrinsic voltage sensitivity of the pore (Fig. 8, A and C). This result suggests a dual role of the VSD, which seems structurally important for the permeation pathway to work, apart from switching between resting to active states to regulate the pore.

DISCUSSION

We report several important insights concerning the novel gating mechanism in K_V10.1 and, possibly, in the

Published March 30, 2017

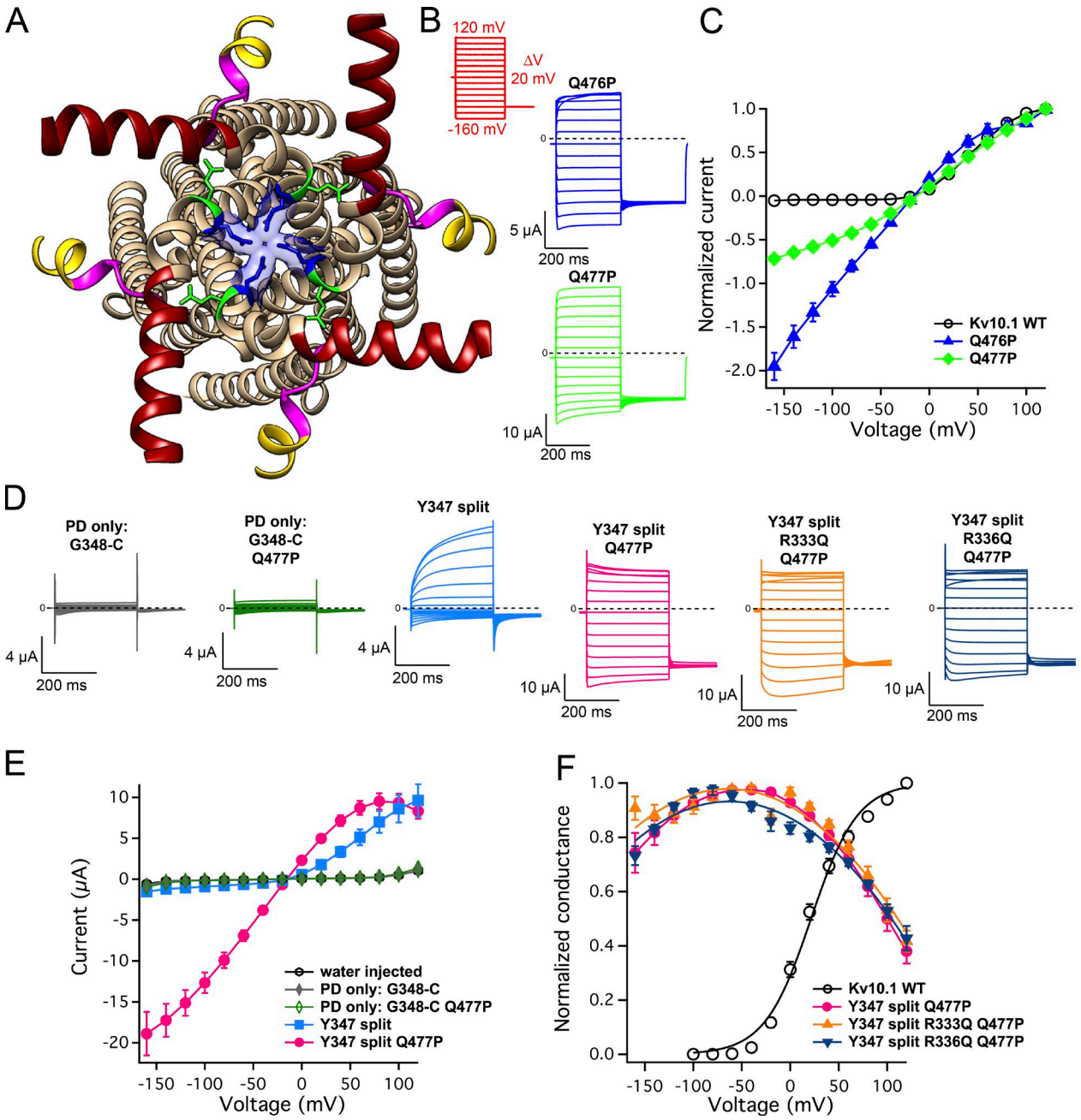

Figure 8. **The presence of VSD is required for a functional permeation pathway even if access to the pore is granted by proline substitutions in S6.** (A) K_V10.1 pore viewed from the intracellular side. The first helix of the C linker is indicated in dark red, Q476 in blue, Q477 in green, the S4–S5 linker in magenta, and the C-terminal S4 in yellow (the part of the helix above the innermost voltage-sensing arginine is not depicted). (B) Representative current traces of Q476P and Q477P mutants in the full-length channel recorded with the indicated voltage protocol. (C) The corresponding normalized, mean current values ± SEM plotted against voltage (n = 5–11). (D) Representative currents from oocytes expressing the isolated PD (G348-C stands for the PD sequence starting from Gly348 and ending at the C terminus), Q477P mutant in the isolated PD, Y347 split and Y347 split carrying Q477P mutation alone, or in combination with additional VSD mutations. (E) Mean current values ± SEM plotted against voltage (n = 7–10; without normalization). (F) Normalized conductance values plotted against voltage. The data represent mean ± SEM (n = 6–10), and the curves are parabola fits for Q477P mutants and a Boltzmann fit for the wild type.

other *KCNH* family channels. First, interrupting the C-terminal S4 helix yields constitutively active channels, whereas breaking a covalent connection in the S4–S5 loop does not. This observation supports the idea that a motion of the C-terminal S4 helix, rather than the S4–S5 linker, closes the channel gate. Second, disconnecting the S4–S5 loop from the S5 helix leads to radical alterations of channel kinetics. It is tempting to specu-

Published March 30, 2017

late that the covalent connection between the S4–S5 loop and the S5 helix is important for orienting the parts of the channel with respect to one another to allow fast gating, without significantly altering the equilibrium energy between the open and the closed conformations. Third, if D342 is mutated to another amino acid except for N, the C-terminal S4 helix can be interrupted with almost complete impunity. Fourth, disconnection between the VSD and the PD does not change VSD motion or changes it only mildly, but the modulation of the channel resting state by prepulse voltage and Mg^{2+} is seriously affected. Finally, the presence of the VSD seems structurally important for the permeation pathway to be functional.

The constitutive activity of the channels interrupted within the C-terminal S4 and the inability of Mg^{2+} and prepulse voltage to slow down their activation kinetics would both point to the conclusion that the C-terminal S4 helix is important for the transition into a stable resting state, as suggested by the interpretation of the available cryo-EM structure (Whicher and MacKinnon, 2016), possibly in a way similar to the hyperpolarization-activated channel HCN (Prole and Yellen, 2006). Our results indicate that the constitutive activity does not arise from a preference of the VSD for the active state and that it requires D342. Further work is needed to identify the interaction partner of D342. Because only the isosteric N could mimic D at this position in the split channel, it is plausible that their side chain carbonyl groups participate as acceptors in a hydrogen bond. Such an interaction would be most compatible with the observation that all the other residues restored channel closure, regardless of their charge, size, or hydrophobicity. We hypothesize that this hydrogen bond could escape the control of the voltage sensor in the split channel, whereas in the full-length channel, it would stabilize the open state when the VSD is in the active position. Along these lines, D342 mutants in the full-length channel show a GV shift to more positive potentials.

In the cryo-EM structure of $K_V10.1$, the side chain of D342 faces open space (Fig. 3 A). However, even though the structure shows the VSD in the active conformation, the channel remains closed. In the open conformation, the position of D342 relative to the other parts of the channel might change. Notably, the available structure does not include the N-terminal tail of the intracellular PAS domain, which influences $K_V10.1$ gating by an interaction with the C-terminal S4 (Terlau et al., 1997). The N-terminal tail could directly interact with the C-terminal S4 helix or the S4–S5 linker or regulate their interaction with other parts of the gating machinery. This hypothesis is supported by the observation that the N-terminal EGFP fusion abolishes the constitutive activity of L341 split (Fig. S7). Interestingly, the D540 residue of $K_V11.1$, which is homologous to D342 in $K_V10.1$, participates in an electrostatic interaction with R665 at the channel gate, stabilizing the closed state (Tristani-Firouzi et al., 2002; Ferrer et al., 2006). This seems unlikely in $K_V10.1$ because the full-length D342 mutants show a preference for the closed state.

The second important insight that comes from our work is the idea that the presence of VSD might be structurally important for the permeation pathway to work, as shown by the experiments using proline substitutions in S6 that lock the channel in the open state. Unless coexpressed with VSD, the pore module of $K_V10.1$ does not conduct even if it also carries Q477P mutation, suggesting that the isolated pore is unable to adopt the conducting conformation without the VSD. Additionally, VSDs with different voltage dependencies can be used in combination with the PD carrying Q477P mutation without changing channel behavior, further indicating that the contribution of VSD is not limited to switching between the resting and the active conformation. For instance, the hydrophobic interaction interface between S1 and S5 could provide a structural scaffold for the PD helices.

Our results also support the view that channel opening and closing are energetically asymmetric, owing to a thermodynamic preference of the pore for the nonconducting state. Such a preference would be compatible with the increased separation between GV and FV curves in Δ342–348 split, where a large part of the coupling interface has been removed, including the bottom of the C-terminal S4 helix. If the role of the C-terminal S4 helix were to close the channel pore at negative potentials, one would expect Δ342–348 split to prefer the open state (assuming that the radical modification that we did to the channel does not alter the intrinsic equilibrium of the pore). Instead, we observed a shift of the GV curve to more positive values. It is also worthwhile to ask which conformation the channel would adopt at 0 mV without the inhibition by Ca^{2+}-Calmodulin. GV plots, in combination with noise analysis recordings performed in our laboratory, allow us to estimate the absolute open probability of the full-length channel at 0 mV to be slightly higher than 0.2, indicating that almost 80% of the channels are closed at any given moment, even though the VSD activation is near-maximal. Collectively, these findings seem to support the experimental studies (Yifrach and MacKinnon, 2002; Pless et al., 2013) and molecular dynamics simulations that suggested an intrinsic preference of the pore for the closed state in eukaryotic channels (Jensen et al., 2010, 2012), whereas the isolated pore modules of voltage-gated bacterial channels prefer the open state (Santos et al., 2008; McCusker et al., 2011, 2012; Shaya et al., 2011; Syeda et al., 2012). Our finding that the C-terminal S4 helix is important for the entry into a stable closed state indicates that the VSD is also needed to maintain the channel closed at negative potentials.

In summary, our data offer partial support to the gating model where the inward motion of the C-terminal S4 helix closes the channel by interacting with the C linker. Although the transition into a stable resting state is affected by interrupting the C-terminal S4 helix, our experiments suggest that channel opening requires more than just release of tension on the C linker. In a more complex picture, VSD motion could change the energy landscape of the channel protein by putting weights on a network of noncovalent interactions between the VSD, the PD, and the intracellular domains. The open probability at any given voltage would then be determined by the weighted mean of the noncovalent interactions (in this scenario, channel opening could happen before all four VSDs are activated, which seems to be the case for L341 split). Gating aberrations in the split channels offer unique opportunities to reveal such interactions and their state dependency, helping to dissect the gating pathway in the *KCNH* channel family. In our split channels, the C-terminal cyclic nucleotide–binding homology domain (CNBHD) together with its intrinsic ligand (Brelidze et al., 2012), which participate in the fast activation of the channel (Zhao et al., 2017), are intact and expected to remain functional. Nevertheless, a change in relative positions of different domains within the molecule cannot be ruled out. Apart from new insights into voltage-gating per se, our work can also help understand mechanistically how gain-of-function mutations that affect the voltage dependency of $K_V10.1$ contribute to severe disease outcomes (Kortüm et al., 2015; Simons et al., 2015; Fukai et al., 2016; Mégarbané et al., 2016).

ACKNOWLEDGMENTS

We thank the expert technical assistance of Annett Sporning, Kerstin Dümke, and Zhu Fu. We are grateful to Michalel Kienzler for the synthesis of glycine maleimide, to Florina Zákány for help in MTS experiments, and to Francisco Barros, Reza Vafabakhsh, Shai Berlin, Raz Palty, and Nathan Dascal for fruitful discussions.

F. Papp and G. Panyi were supported by the Hungarian Brain Research Program (KTIA_NAP_13-2-2015-0009).

The authors declare no competing financial interests.

Richard W. Aldrich served as editor.

Submitted: 15 December 2016
Revised: 9 February 2017
Accepted: 16 February 2017

REFERENCES

Armstrong, C.M., and F. Bezanilla. 1973. Currents related to movement of the gating particles of the sodium channels. *Nature.* 242:459–461. http://dx.doi.org/10.1038/242459a0

Brelidze, T.I., A.E. Carlson, B. Sankaran, and W.N. Zagotta. 2012. Structure of the carboxy-terminal region of a KCNH channel. *Nature.* 481:530–533. http://dx.doi.org/10.1038/nature10735

Chanda, B., O.K. Asamoah, R. Blunck, B. Roux, and F. Bezanilla. 2005. Gating charge displacement in voltage-gated ion channels involves limited transmembrane movement. *Nature.* 436:852–856. http://dx.doi.org/10.1038/nature03888

Chowdhury, S., and B. Chanda. 2012. Perspectives on: Conformational coupling in ion channels: Thermodynamics of electromechanical coupling in voltage-gated ion channels. *J. Gen. Physiol.* 140:613–623. http://dx.doi.org/10.1085/jgp.201210840

Ferrer, T., J. Rupp, D.R. Piper, and M. Tristani-Firouzi. 2006. The S4-S5 linker directly couples voltage sensor movement to the activation gate in the human ether-a'-go-go-related gene (hERG) K^+ channel. *J. Biol. Chem.* 281:12858–12864. http://dx.doi.org/10.1074/jbc.M513518200

Fukai, R., H. Saitsu, Y. Tsurusaki, Y. Sakai, K. Haginoya, K. Takahashi, M.W. Hubshman, N. Okamoto, M. Nakashima, F. Tanaka, et al. 2016. De novo KCNH1 mutations in four patients with syndromic developmental delay, hypotonia and seizures. *J. Hum. Genet.* 61:381–387. http://dx.doi.org/10.1038/jhg.2016.1

Gandhi, C.S., E. Clark, E. Loots, A. Pralle, and E.Y. Isacoff. 2003. The orientation and molecular movement of a K^+ channel voltage-sensing domain. *Neuron.* 40:515–525. http://dx.doi.org/10.1016/S0896-6273(03)00646-9

Hemmerlein, B., R.M. Weseloh, F. Mello de Queiroz, H. Knötgen, A. Sánchez, M.E. Rubio, S. Martin, T. Schliephacke, M. Jenke, Heinz-Joachim-Radzun, et al. 2006. Overexpression of Eag1 potassium channels in clinical tumours. *Mol. Cancer.* 5:41. http://dx.doi.org/10.1186/1476-4598-5-41

Hille, B. 2001. Ion Channels of Excitable Membranes. Third edition. Sinauer Associates, Sunderland, MA. 814 pp.

Isacoff, E.Y., L.Y. Jan, and D.L. Minor Jr. 2013. Conduits of life's spark: a perspective on ion channel research since the birth of neuron. *Neuron.* 80:658–674. http://dx.doi.org/10.1016/j.neuron.2013.10.040

Jensen, M.O., D.W. Borhani, K. Lindorff-Larsen, P. Maragakis, V. Jogini, M.P. Eastwood, R.O. Dror, and D.E. Shaw. 2010. Principles of conduction and hydrophobic gating in K^+ channels. *Proc. Natl. Acad. Sci. USA.* 107:5833–5838. http://dx.doi.org/10.1073/pnas.0911691107

Jensen, M.O., V. Jogini, D.W. Borhani, A.E. Leffler, R.O. Dror, and D.E. Shaw. 2012. Mechanism of voltage gating in potassium channels. *Science.* 336:229–233. http://dx.doi.org/10.1126/science.1216533

Jiang, Y., V. Ruta, J. Chen, A. Lee, and R. MacKinnon. 2003. The principle of gating charge movement in a voltage-dependent K^+ channel. *Nature.* 423:42–48. http://dx.doi.org/10.1038/nature01581

Kortüm, F., V. Caputo, C.K. Bauer, L. Stella, A. Ciolfi, M. Alawi, G. Bocchinfuso, E. Flex, S. Paolacci, M.L. Dentici, et al. 2015. Mutations in KCNH1 and ATP6V1B2 cause Zimmermann-Laband syndrome. *Nat. Genet.* 47:661–667. http://dx.doi.org/10.1038/ng.3282

Labro, A.J., A.L. Raes, A. Grottesi, D. Van Hoorick, M.S.P. Sansom, and D.J. Snyders. 2008. Kv channel gating requires a compatible S4-S5 linker and bottom part of S6, constrained by non-interacting residues. *J. Gen. Physiol.* 132:667–680. http://dx.doi.org/10.1085/jgp.200810048

Labro, A.J., I.R. Boulet, F.S. Choveau, E. Mayeur, T. Bruyns, G. Loussouarn, A.L. Raes, and D.J. Snyders. 2011. The S4-S5 linker of KCNQ1 channels forms a structural scaffold with the S6 segment controlling gate closure. *J. Biol. Chem.* 286:717–725. http://dx.doi.org/10.1074/jbc.M110.146977

Long, S.B., E.B. Campbell, and R. Mackinnon. 2005a. Crystal structure of a mammalian voltage-dependent Shaker family K^+ channel. *Science.* 309:897–903. http://dx.doi.org/10.1126/science.1116269

Long, S.B., E.B. Campbell, and R. Mackinnon. 2005b. Voltage sensor of Kv1.2: structural basis of electromechanical coupling. *Science.* 309:903–908. http://dx.doi.org/10.1126/science.1116270

Long, S.B., X. Tao, E.B. Campbell, and R. MacKinnon. 2007. Atomic structure of a voltage-dependent K^+ channel in a lipid membrane-like environment. *Nature.* 450:376–382. http://dx.doi.org/10.1038/nature06265

Lörinczi, É., J.C. Gómez-Posada, P. de la Peña, A.P. Tomczak, J. Fernández-Trillo, U. Leipscher, W. Stühmer, F. Barros, and L.A. Pardo. 2015. Voltage-dependent gating of KCNH potassium channels lacking a covalent link between voltage-sensing and pore domains. *Nat. Commun.* 6:6672. http://dx.doi.org/10.1038/ncomms7672

Lu, Z., A.M. Klem, and Y. Ramu. 2002. Coupling between voltage sensors and activation gate in voltage-gated K^+ channels. *J. Gen. Physiol.* 120:663–676. http://dx.doi.org/10.1085/jgp.20028696

Ludwig, J., H. Terlau, F. Wunder, A. Brüggemann, L.A. Pardo, A. Marquardt, W. Stühmer, and O. Pongs. 1994. Functional expression of a rat homologue of the voltage gated either á go-go potassium channel reveals differences in selectivity and activation kinetics between the *Drosophila* channel and its mammalian counterpart. *EMBO J.* 13:4451–4458.

Macdonald, P.J., Y. Chen, and J.D. Mueller. 2012. Chromophore maturation and fluorescence fluctuation spectroscopy of fluorescent proteins in a cell-free expression system. *Anal. Biochem.* 421:291–298. http://dx.doi.org/10.1016/j.ab.2011.10.040

McCusker, E.C., N. D'Avanzo, C.G. Nichols, and B.A. Wallace. 2011. Simplified bacterial "pore" channel provides insight into the assembly, stability, and structure of sodium channels. *J. Biol. Chem.* 286:16386–16391. http://dx.doi.org/10.1074/jbc.C111.228122

McCusker, E.C., C. Bagnéris, C.E. Naylor, A.R. Cole, N. D'Avanzo, C.G. Nichols, and B.A. Wallace. 2012. Structure of a bacterial voltage-gated sodium channel pore reveals mechanisms of opening and closing. *Nat. Commun.* 3:1102. http://dx.doi.org/10.1038/ncomms2077

Mégarbané, A., R. Al-Ali, N. Choucair, M. Lek, E. Wang, M. Ladjimi, C.M. Rose, R. Hobeika, Y. Macary, R. Temanni, et al. 2016. Temple-Baraitser Syndrome and Zimmermann-Laband Syndrome: one clinical entity? *BMC Med. Genet.* 17:42. http://dx.doi.org/10.1186/s12881-016-0304-4

Mortensen, L.S., H. Schmidt, Z. Farsi, A. Barrantes-Freer, M.E. Rubio, R. Ufartes, J. Eilers, T. Sakaba, W. Stühmer, and L.A. Pardo. 2015. KV 10.1 opposes activity-dependent increase in Ca^{2+} influx into the presynaptic terminal of the parallel fibre-Purkinje cell synapse. *J. Physiol.* 593:181–196. http://dx.doi.org/10.1113/jphysiol.2014.281600

Padilla-Parra, S., N. Audugé, H. Lalucque, J.-C. Mevel, M. Coppey-Moisan, and M. Tramier. 2009. Quantitative comparison of different fluorescent protein couples for fast FRET-FLIM acquisition. *Biophys. J.* 97:2368–2376. http://dx.doi.org/10.1016/j.bpj.2009.07.044

Papazian, D.M., L.C. Timpe, Y.N. Jan, and L.Y. Jan. 1991. Alteration of voltage-dependence of Shaker potassium channel by mutations in the S4 sequence. *Nature.* 349:305–310. http://dx.doi.org/10.1038/349305a0

Pardo, L.A., D. del Camino, A. Sánchez, F. Alves, A. Brüggemann, S. Beckh, and W. Stühmer. 1999. Oncogenic potential of EAG K^+ channels. *EMBO J.* 18:5540–5547. http://dx.doi.org/10.1093/emboj/18.20.5540

Payandeh, J., T. Scheuer, N. Zheng, and W.A. Catterall. 2011. The crystal structure of a voltage-gated sodium channel. *Nature.* 475:353–358. http://dx.doi.org/10.1038/nature10238

Pless, S.A., A.P. Niciforovic, J.D. Galpin, J.-J. Nunez, H.T. Kurata, and C.A. Ahern. 2013. A novel mechanism for fine-tuning open-state stability in a voltage-gated potassium channel. *Nat. Commun.* 4:1784. http://dx.doi.org/10.1038/ncomms2761

Posson, D.J., P. Ge, C. Miller, F. Bezanilla, and P.R. Selvin. 2005. Small vertical movement of a K^+ channel voltage sensor measured with luminescence energy transfer. *Nature.* 436:848–851. http://dx.doi.org/10.1038/nature03819

Prole, D.L., and G. Yellen. 2006. Reversal of HCN channel voltage dependence via bridging of the S4-S5 linker and Post-S6. *J. Gen. Physiol.* 128:273–282. http://dx.doi.org/10.1085/jgp.200609590

Ruta, V., J. Chen, and R. MacKinnon. 2005. Calibrated measurement of gating-charge arginine displacement in the K_vAP voltage-dependent K^+ channel. *Cell.* 123:463–475. http://dx.doi.org/10.1016/j.cell.2005.08.041

Sánchez, A., D. Urrego, and L.A. Pardo. 2016. Cyclic expression of the voltage-gated potassium channel $K_V10.1$ promotes disassembly of the primary cilium. *EMBO Rep.* 17:708–723. http://dx.doi.org/10.15252/embr.201541082

Sanguinetti, M.C., and Q.P. Xu. 1999. Mutations of the S4-S5 linker alter activation properties of HERG potassium channels expressed in Xenopus oocytes. *J. Physiol.* 514:667–675. http://dx.doi.org/10.1111/j.1469-7793.1999.667ad.x

Santos, J.S., S.M. Grigoriev, and M. Montal. 2008. Molecular template for a voltage sensor in a novel K^+ channel. III. Functional reconstitution of a sensorless pore module from a prokaryotic K_v channel. *J. Gen. Physiol.* 132:651–666. http://dx.doi.org/10.1085/jgp.200810077

Schönherr, R., L.M. Mannuzzu, E.Y. Isacoff, and S.H. Heinemann. 2002. Conformational switch between slow and fast gating modes: allosteric regulation of voltage sensor mobility in the EAG K^+ channel. *Neuron.* 35:935–949. http://dx.doi.org/10.1016/S0896-6273(02)00869-3

Shaya, D., M. Kreir, R.A. Robbins, S. Wong, J. Hammon, A. Brüggemann, and D.L. Minor Jr. 2011. Voltage-gated sodium channel (Na_V) protein dissection creates a set of functional pore-only proteins. *Proc. Natl. Acad. Sci. USA.* 108:12313–12318. http://dx.doi.org/10.1073/pnas.1106811108

Silverman, W.R., C.Y. Tang, A.F. Mock, K.B. Huh, and D.M. Papazian. 2000. Mg^{2+} modulates voltage-dependent activation in ether-à-go-go potassium channels by binding between transmembrane segments S2 and S3. *J. Gen. Physiol.* 116:663–678. http://dx.doi.org/10.1085/jgp.116.5.663

Simons, C., L.D. Rash, J. Crawford, L. Ma, B. Cristofori-Armstrong, D. Miller, K. Ru, G.J. Baillie, Y. Alanay, A. Jacquinet, et al. 2015. Mutations in the voltage-gated potassium channel gene *KCNH1* cause Temple-Baraitser syndrome and epilepsy. *Nat. Genet.* 47:73–77. http://dx.doi.org/10.1038/ng.3153

Slesinger, P.A., Y.N. Jan, and L.Y. Jan. 1993. The S4-S5 loop contributes to the ion-selective pore of potassium channels. *Neuron.* 11:739–749. http://dx.doi.org/10.1016/0896-6273(93)90083-4

Stühmer, W., F. Conti, H. Suzuki, X.D. Wang, M. Noda, N. Yahagi, H. Kubo, and S. Numa. 1989. Structural parts involved in activation and inactivation of the sodium channel. *Nature.* 339:597–603. http://dx.doi.org/10.1038/339597a0

Syeda, R., J.S. Santos, M. Montal, and H. Bayley. 2012. Tetrameric assembly of K_vLm K^+ channels with defined numbers of voltage sensors. *Proc. Natl. Acad. Sci. USA.* 109:16917–16922. http://dx.doi.org/10.1073/pnas.1205592109

Terlau, H., S.H. Heinemann, W. Stühmer, O. Pongs, and J. Ludwig. 1997. Amino terminal-dependent gating of the potassium channel rat eag is compensated by a mutation in the S4 segment. *J. Physiol.* 502:537–543. http://dx.doi.org/10.1111/j.1469-7793.1997.537bj.x

Thouta, S., S. Sokolov, Y. Abe, S.J. Clark, Y.M. Cheng, and T.W. Claydon. 2014. Proline scan of the HERG channel S6 helix reveals the location of the intracellular pore gate. *Biophys. J.* 106:1057–1069. http://dx.doi.org/10.1016/j.bpj.2014.01.035

Tombola, F., M.M. Pathak, and E.Y. Isacoff. 2005. Voltage-sensing arginines in a potassium channel permeate and occlude cation-selective pores. *Neuron*. 45:379–388. http://dx.doi.org/10.1016/j.neuron.2004.12.047

Tristani-Firouzi, M., J. Chen, and M.C. Sanguinetti. 2002. Interactions between S4-S5 linker and S6 transmembrane domain modulate gating of HERG K^+ channels. *J. Biol. Chem.* 277:18994–19000. http://dx.doi.org/10.1074/jbc.M200410200

Ulbrich, M.H., and E.Y. Isacoff. 2007. Subunit counting in membrane-bound proteins. *Nat. Methods*. 4:319–321.

Urrego, D., N. Movsisyan, R. Ufartes, and L.A. Pardo. 2016. Periodic expression of Kv10.1 driven by pRb/E2F1 contributes to G2/M progression of cancer and non-transformed cells. *Cell Cycle*. 15:799–811. http://dx.doi.org/10.1080/15384101.2016.1138187

Van Slyke, A.C., S. Rezazadeh, M. Snopkowski, P. Shi, C.R. Allard, and T.W. Claydon. 2010. Mutations within the S4–S5 linker alter voltage sensor constraints in hERG K^+ channels. *Biophys. J.* 99:2841–2852. http://dx.doi.org/10.1016/j.bpj.2010.08.030

Vargas, E., V. Yarov-Yarovoy, F. Khalili-Araghi, W.A. Catterall, M.L. Klein, M. Tarek, E. Lindahl, K. Schulten, E. Perozo, F. Bezanilla, and B. Roux. 2012. An emerging consensus on voltage-dependent gating from computational modeling and molecular dynamics simulations. *J. Gen. Physiol.* 140:587–594. http://dx.doi.org/10.1085/jgp.201210873

Whicher, J.R., and R. MacKinnon. 2016. Structure of the voltage-gated K^+ channel Eag1 reveals an alternative voltage sensing mechanism. *Science*. 353:664–669. http://dx.doi.org/10.1126/science.aaf8070

Yifrach, O., and R. MacKinnon. 2002. Energetics of pore opening in a voltage-gated K^+ channel. *Cell*. 111:231–239. http://dx.doi.org/10.1016/S0092-8674(02)01013-9

Zhao, Y., M.P. Goldschen-Ohm, J.H. Morais-Cabral, B. Chanda, and G.A. Robertson. 2017. The intrinsically liganded cyclic nucleotide-binding homology domain promotes KCNH channel activation. *J. Gen. Physiol.* 149:249–260. http://dx.doi.org/10.1085/jgp.201611701